The Journal of Experimental Biology 216, 3023-3034

doi:10.1242/jeb.084822

RESEARCH ARTICLE

Environmental response and adaptation of glycoprotein glue within the droplets of viscous prey capture threads from araneoid spider orb-webs

Brent D. Opell*, Shannon E. Karinshak and Mary A. Sigler
Department of Biological Sciences, Virginia Tech, Blacksburg, VA 24061, USA
*Author for correspondence (bopell@vt.edu)

SUMMARY

Viscous threads that form the prey capture spiral of araneoid orb-webs retain insects that strike the web, giving a spider more time to locate and subdue them. The viscoelastic glycoprotein glue responsible for this adhesion forms the core of regularly spaced aqueous droplets, which are supported by protein axial fibers. Glycoprotein extensibility both facilitates the recruitment of adhesion from multiple droplets and dissipates the energy generated by insects struggling to free themselves from the web. Compounds in the aqueous material make the droplets hygroscopic, causing an increase in both droplet volume and extensibility as humidity (RH) rises. We characterized these humidity-mediated responses at 20%, 37%, 55%, 72% and 90% RH in two large orb-weavers, *Argiope aurantia*, which is found in exposed habitats, and *Neoscona crucifera*, which occupies forests and forest edges. The volume-specific extension of *A. aurantia* glycoprotein reached a maximum value at 55% RH and then declined, whereas that of *N. crucifera* increased exponentially through the RH range. As RH increased, the relative stress on droplet filaments at maximum extension, as gauged by axial line deflection, decreased in a linear fashion in *A. aurantia*, but in *N. crucifer* increased logarithmically, indicating that *N. crucifera* threads are better equipped to dissipate energy through droplet elongation. The greater hygroscopicity of *A. aurantia* threads equips them to function in lower RH environments and during the afternoon when RH drops, but their performance is diminished during the high RH of the morning hours. In contrast, the lower hygroscopicity of *N. crucifera* threads optimizes their performance for intermediate and high RH environments and during the night and morning. These interspecific differences support the hypothesis that viscous capture threads are adapted to the humidity regime of an orb-weaver's habitat.

Key words: Araneoidea, *Argiope aurantia*, biomaterial, glycoprotein, hygroscopic, *Neoscona crucifera*.

Received 2 January 2013; Accepted 12 April 2013

INTRODUCTION

Many biological materials respond in adaptive ways to environmental humidity. For example, keratin in gecko toe pads softens as humidity rises to increase toe adhesion (Puthoff et al., 2010) and wheat awns shrink and swell cyclically with humidity changes, burying seeds in the soil (Elbaum et al., 2007). High humidity during the late evening or early morning hours when most orb-weaving spiders construct their webs is crucial for configuring a web's prey capture threads (Fig. 1) (Peters, 1986; Vollrath, 1992). These sticky threads form the web's capture spiral, which retains insects that strike the web, giving a spider more time to locate and subdue these prey before they escape from the web (Blackledge and Zevenbergen, 2006; Chacón and Eberhard, 1980). The material that forms these viscous threads issues from three spinning spigots on each of the spider's paired posterior spinnerets: a flagelliform gland that spins a supporting protein axial fiber and two aggregate glands that coat this fiber with an aqueous solution (Coddington, 1989). When these coated fibers first merge to form a thread, their aqueous covering forms a continuous cylinder. Salts and as many as 12 low molecular weight compounds, such as GABamide, glycine and choline (Edmonds and Vollrath, 1992; Fisher and Brander, 1960; Higgins et al., 2001; Townley et al., 1991; Tillinghast and Christenson, 1984; Townley et al., 2006; Vollrath et al., 1990) make this coating hygroscopic, causing it to rapidly absorb atmospheric moisture and be reconfigured by Rayleigh instability into droplets (Edmonds and Vollrath, 1992). Within each droplet, ASG1 and ASG2 glycoproteins condense into a viscoelastic core that is both adhesive and extensible (Choresh et al., 2009; Sahni et al., 2010; Tillinghast et al., 1993; Townley et al., 2006), properties that combine to generate an effective adhesive delivery system (Opell and Hendricks, 2007; Opell and Hendricks, 2009). The ASG1 protein contains a non-repetitive region rich in charged amino acids and is considered to be hydrophilic (Choresh et al., 2009).

This hygroscopic legacy continues to impact a viscous thread over the course of a day. Both the volume and extensibility of *Larinoides cornutus* thread droplets are directly related to relative humidity (RH) (Opell et al., 2011a). The extension bridge mechanism by which viscous threads sum the adhesion of multiple droplets relies on droplet extensibility (Opell and Hendricks, 2007; Opell and Hendricks, 2009). Therefore, these humidity changes have the potential to alter viscous thread adhesion. Thread adhesion can be gauged in two ways: the force required to pull a thread from a surface (e.g. Agnarsson and Blackledge, 2009; Opell and Hendricks, 2009) and the energy required to do so (Sahni et al., 2011). The latter value gauges a thread's ability to dissipate the force of an insect struggling to free itself from a web. At rapid extension velocities, an increase in RH from 15% to 40% resulted in a 360% increase in the energy required to pull *L. cornutus* viscous threads from a surface. However, this energy decreased by 67% at 90% RH, indicating that water uptake at intermediate humidity

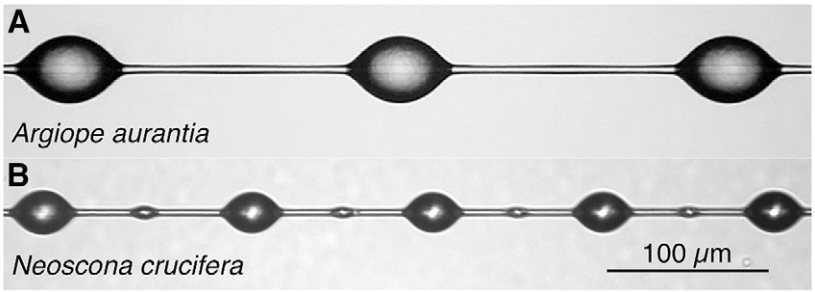

Fig. 1. Viscous threads of *Argiope aurantia* (A) and *Neoscona crucifera* (B), at the same magnification.

optimized glycoprotein performance, whereas at higher humidity excess water over-lubricated the glycoprotein, causing it to more easily pull from a surface (Sahni et al., 2011).

As a viscous thread's response to humidity has the potential to significantly affect thread performance, we hypothesized that selection has optimized thread hygroscopicity to the humidity regime of a species' habitat. To test this hypothesis and to more fully characterize the humidity responses of viscous thread droplets, we examined the performance of threads spun by two species: *Argiope aurantia* Lucas 1833, a species commonly found in exposed, weedy vegetation (Carrel, 2008; Enders, 1977; Young and Edwards, 1990), and *Neoscona crucifera* (Lucas 1839), a species that builds its webs in forests and along forest edges (Adams, 2000; Edwards, 1984). *Neoscona crucifera* can both be nocturnal and continue to use its webs during daylight hours. We hypothesized that the viscous droplets of *A. aurantia* are more hygroscopic than those of *N. crucifera*, permitting them to remain optimally hydrated during the drier times of the day. We tested this hypothesis by using an expanded number of experimental humidities (20%, 37%, 55%, 72% and 90% RH) that permitted us to more fully characterize droplet response (Fig. 2) and a new technique that permitted us to visualize (Fig. 3) and quantify a droplet's glycoprotein core and to compute glycoprotein volume-specific indices of droplet extension (Fig. 4).

MATERIALS AND METHODS

Collecting viscous thread samples

We collected viscous threads from orb-webs constructed by 14 adult females of each species between 06:00 h and 08:00 h from sites near Blacksburg, Montgomery County, VA, USA, from 29 August to 30 September 2011. *Argiope aurantia* threads were collected from webs constructed in weedy vegetation along the margins of a meadow (Heritage Park) and *N. crucifera* threads from trees and shrubs along the edge of a forest adjacent to a Virginia Tech agricultural field. A Hobo data logger at each site recorded humidity at 10 min intervals during the 33 days that web samples were collected. To prevent theft, the data logger at the *A. aurantia* site was situated in an area where the surrounding vegetation probably maintained humidity at higher levels throughout the day than in more exposed places where many *A. aurantia* were found. Therefore, the humidity reported for this habitat is probably higher than some or many *A. aurantia* experience.

Samples of two individuals' webs were collected on each study day and the positions of these webs marked with flagging tape to prevent resampling. Images and videos from which measurements of droplet extension were later made were completed by 12:00 h and photographs used to determine glycoprotein area were completed by 16:00 h of the same day. To minimize temporal effects, we alternated the species studied, characterizing the threads of 2–4 individuals of one species and then switching to the other.

We collected an orb-web sector on a 17 cm diameter aluminum ring with a bar across its center. Scotch double-coated tissue tape (Tape 4101T; 3M, St Paul, MN, USA) applied to the 5 mm wide rim of the ring and bar secured threads at their native tensions. After transporting web samples to the laboratory in a closed container, we placed 4 mm wide brass bars covered with double-sided carbon tape (product 77816, Electron Microscopy Sciences, Hatfield, PA, USA) across the ring's center bar and rim along the sample's radial threads. This allowed us to collect short spans of capture thread

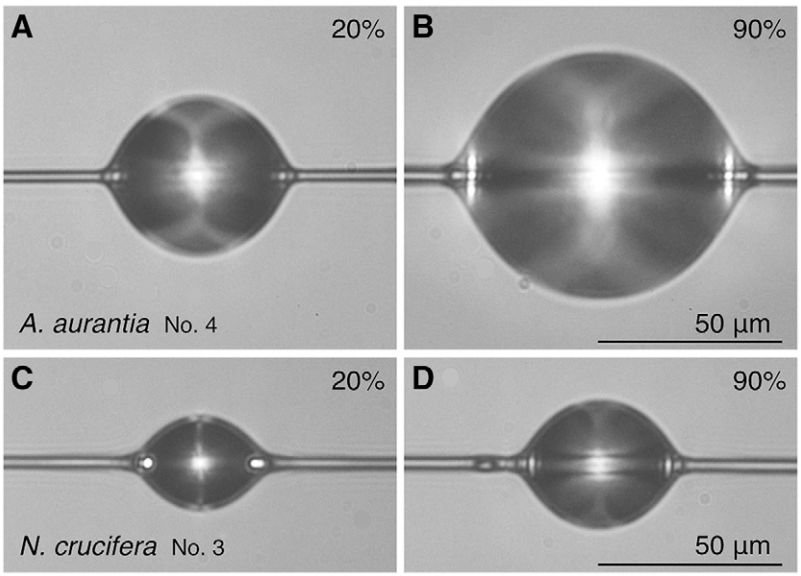

Fig. 2. Viscous thread droplets of *A. aurantia* (A,B) and *N. crucifera* (C,D) at 20% relative humidity (RH; A,C) and 90% RH (B,D), at the same magnification.

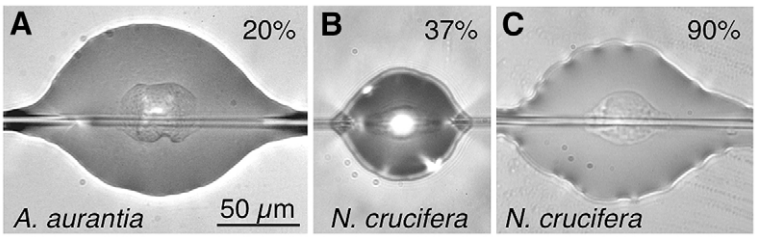

Fig. 3. Flattened droplets of *A. aurantia* (A) and *N. crucifera* (B,C) showing the glycoprotein core of each droplet at 20% RH (A), 37% RH (B) and 90% RH (C), at the same magnification.

without damaging other regions of the web sample or altering the native tension of adjacent viscous threads. We then collected individual threads from the outer third of an orb-web's capture region using a pair of tweezers whose tips were covered with double-sided carbon tape and blocked open to accommodate the support spacing of thread samplers. We accomplished this by pressing the tweezer tips against a thread and cutting it free using iris scissors. This thread sector was then transferred to the carbon tape-covered rails of adjacent brass, U-shaped supports glued at 4.8 mm intervals to a microscope slide to form a thread sampler [see fig. 3 in Opell et al. (Opell et al., 2011b)].

As adjacent droplets usually merged upon contacting the tip of the probe used to extend a droplet, we isolated an individual thread droplet near the center of each 4.8 mm long thread span. Exhaling gently on a thread span temporarily more fully hydrated its droplets, allowing unwanted droplets to be pushed away from the focal droplet using the moistened tip of a probe made from an insect minuten pin. This procedure did not remove the thin aqueous layer that covers axial fibers in inter-droplet regions and maintains their supercontraction. After droplets were moved, small secondary droplets, like those often found between the large primary droplets of native threads (Fig. 1B), reformed in the regions where larger droplets had been.

Controlling humidity and observing threads

To control RH, we placed thread samplers in a humidity chamber [see fig. 4 in Opell et al. (Opell et al., 2011a)], which incorporated a holder for the thread sampler and ports for air inlet and outlet tubes, the droplet extension probe and the probe of a Fisher Scientific Instant Digital Hygrometer (Waltham, MA, USA), whose readings were updated in less than 10 s. A sheet of anti-Newton glass resting on a Sorbothane gasket sealed the top of this aluminum chamber. We controlled humidity by placing a small Petri dish filled with either silica gel beads or a Kimwipe moistened with distilled water into the chamber. Humidity was then adjusted by either exhaling into a tube connected to a chamber port to introduced humid air or withdrawing air from the tube to introduce drier room air. Temperature within the chamber was maintained at 23–24°C. Samples were measured first at 20% RH and then at successively higher values (37%, 55%, 72% and 90%). As described below, three sets of measurements were required to assemble this study's data. Our ability to establish RH values within tight limits resulted in the five experimental RH values being nearly identical for each set of the three measurement sets (Table 1).

Measuring droplet dimensions and extension

At each humidity a different isolated, suspended droplet from a spider's web was photographed (Fig. 2) with a Canon T1i digital camera attached to a Mitutoyo FS60 inspection microscope. An image of a stage micrometer taken at the same magnification served as a scale for measuring suspended droplet length (DL, dimension parallel to the thread's axial fibers) and droplet width (DW) with ImageJ (Rasband, 1997-2012). Following an earlier study (Opell and Schwend, 2007), we computed droplet volume (DV) according to the following formula for a parabolic volume:

$$DV = (2\pi \times DW^2 \times DL) / 15 . \quad (1)$$

After photographing a suspended droplet, we extended it using procedures that are described in detail a previous paper (Opell et al., 2011a) while a video was recorded at 60 frames s^{-1}. Before each trial we used 95% ethanol on a Kimwipe to clean the flat tip of the single steel probe, which was used to contact and extend all droplets. This probe was inserted through a port in the side of the chamber, and its tip was aligned with and then brought into contact with the droplet, advanced 500 μm to firmly attach the glycoprotein core to the probe's flat tip, and then withdrawn from the droplet at a velocity of 69.5 μm s^{-1}, while a video was recorded. The last video frame in which the extending droplet was attached to the probe's tip was captured (Fig. 4) and the length of the droplet filament measured with ImageJ using the probe's 413 μm wide tip as a scale.

The axial lines supporting some droplets at high humidities extended beyond the camera's field of view, although in all instances we were able to observe the extending filament and identify a droplet's release from the probe. In these cases we used the position of the time scale slider bar at the bottom of the video frame to determine droplet extension. We first screened captured images of

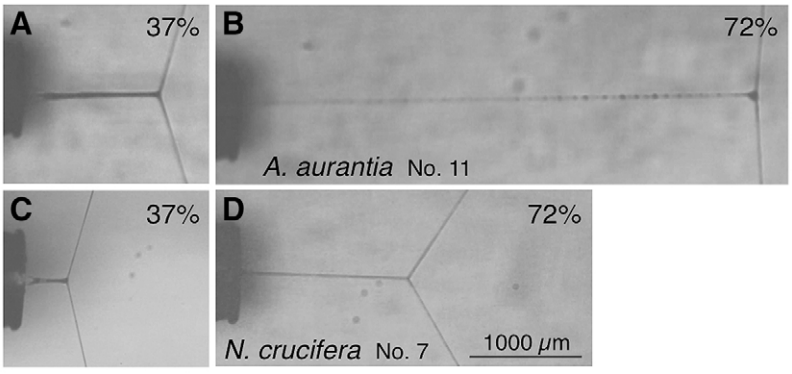

Fig. 4. Extended droplets of *A. aurantia* (A,B) and *N. crucifera* (C,D) at their maximum lengths prior to pull-off at 37% RH (A,C) and 72% RH (B,D), at the same magnification.

Table 1. Features of *Argiope aurantia* and *Neoscona crucifera* droplets and the humidities at which they were measured

	Argiope aurantia					*Neoscona crucifera*				
	20%	37%	55%	72%	90%	20%	37%	55%	72%	90%
Humidity										
Suspended	20.4±0.2	37.2±0.1	55.1±0.1	72.1±0.1	90.2±0.2	20.8±0.3	37.0±0.1	55.3±0.2	72.0±0.1	90.1±0.1
Flattened	20.7±0.2	37.2±0.1	55.5±0.1	71.9±0.2	90.4±0.3	21.1±0.7	37.0±0.2	55.1±0.2	72.1±0.2	90.0±0.1
Extended	20.1±0.4	37.0±0.2	55.1±0.1	71.9±0.1	90.1±0.	20.4±0.4	36.7±0.2	55.4±0.1	72.1±0.2	90.1±0.1
Droplet										
Length (µm)	62±3	65±4	65±4	69±4	80±4	41±2	38±2	38±2	42±2	45±2
Width (µm)	45±3	48±3	49±3	51±3	61±3	29±1	27±1	29±1	32±1	34±1
Volume (µm^3)	59,526±9221	69,956±11,532	74,907±12,954	82,840±14,754	138,353±19,089	15,362±2053	12,695±1746	14,973±2055	19,336±2731	23,557±2654
Flat area (µm^2)	9193±1582	11,217±1111	12,964±1703	16,968±3290	21,052±2723	1107±225	2009±269	3218±319	4948±480	5273±603
Flat thickness (µm)	7.26±1.01	5.95±0.58	5.54±0.55	5.26±0.51	6.65±0.59	17.20±6.55	7.75±1.24	4.56±0.27	3.74±0.25	4.65±0.39
Aqueous vol. (µm^3)	49,966±7460	58,910±9961	65,865±11,352	75,263±15,458	121,460±17,275	[8900]	11,079±1342	13,363±1842	17,119±2682	20,993±2356
Glycoprotein										
Flat area (µm^2)	1328±185	1744±185	1477±187	2149±431	3110±378	–	379±82	409±51	518±48	572±78
Volume (µm^3)	9561±1880	11,046±1882	9042±1711	11,614±2930	21,090±3097	[1270]	1875±341	1948±362	1992±274	2563±339
% Aqueous vol.	18.59±1.67	20.00±2.55	13.35±0.99	14.63±1.13	17.51	[23.45]	18.10±4.09	13.84±0.97	11.77±0.46	12.16±0.71
Extension										
Drop vol. (µm^3)	68,875±11,476	82,082±16,258	86,126±16,474	98,485±18,798	160,479±26,649	16,179±3079	15,190±2479	19,591±4150	22,356±4615	32,672±5240
Glycoprotein vol. (µm^3)	11,003±2180	12,973±2424	10,597±2350	14,680±4189	24,564±4311	–	2189±589	2625±696	2277±419	3504±597
Extension (µm)	561±72	1771±240	2796±700	3410±767	4266±557	49±16	151±25	472±67	1297±215	3984±898
EGV (µm µm^{-3})	0.071±0.014	0.200±0.043	0.368±0.077	0.339±0.066	0.232±0.043	[0.053]	0.128±0.030	0.252±0.044	0.643±0.077	1.318±0.272

Data are means ± 1 s.e.m.
Exension glycoprotein volumes are inferred. EGV, extension per (inferred) glycoprotein volume.
For *N. crucifera*, values inferred for 20% RH from regression plots are given in brackets.

an extending droplet at the same enlargement at three points during droplet extension: T1, the point just before droplet extension; T2, the point at which the axial line disappeared from the frame; and T3, the point at which the droplet filament was released from the probe tip. We then measured the position of the slider with a digital caliper to an accuracy of 0.5 mm. For an average *A. aurantia* out-of-frame droplet extension, measurements were obtained to an accuracy of ±2%, ±0.6% and ±0.5% for positions T1, T2 and T3, respectively. We also measured the length of the droplet filament at time T2 (L1). For an average *A. aurantia* out-of-frame droplet extension, this was done to an accuracy of ±20 µm or ±0.6% L1 filament length. The length of droplet extension (DE) at pull-off from the probe tip was computed as:

$$DE = [L1 / (T2 - T1)] \times (T3 - T1). \quad (2)$$

For a representative *A. aurantia* out-of-frame droplet extension at 90% RH, the combination of measurement inaccuracies that produced the most extreme DE values resulted in a maximum deviation of ±161 µm or 3.7% of the median DE computed for this individual.

Determining glycoprotein volume

The glycoprotein core of droplets becomes visible when a glass coverslip is placed on a thread that is suspended between the supports of a thread sampler (Fig. 3). Unlike similar preparations viewed with a standard compound microscope (Fig. 5A) (Opell and Hendricks, 2010), the epi-illumination of the Mitutoyo microscope used in this study resolved the glycoprotein's outline, but did not reveal the smaller granule at its center (Fig. 3). To flatten droplets without opening the chamber after a desired RH was established and suspended droplets were photographed, a 22 mm diameter glass coverslip was suspended over the thread in a device attached by magnets to the underside of the chamber's glass cover. After three suspended droplets were photographed through the coverslip and their positions recorded, a magnet triggered the coverslip's release onto the suspended thread. All coverslips used to flatten droplets

Fig. 5. Flattened viscous thread and water droplets on glass. *Argiope aurantia* droplet at 50% RH viewed with Nomarski optics (A), a side view of a distilled water droplet (B) and a side view of a flattened viscous droplet modeled on a distilled water droplet (C).

came from the same box and each was cleaned with a Kimwipe moistened with 95% ethanol immediately before use.

To ensure that the coverslip was firmly and uniformly pressed against the droplets, a probe was inserted through the port in the side of the chamber, positioned over the coverslip and centered between the supports of the microscope slide sampler, on which the coverslip rested. The shaft of the probe was then pressed downward until its movement was stopped by the lower edge of the slit in the chamber's side that permitted the probe to be moved along the length of the chamber for alignment with the droplets. Thus, we believe that the force applied in flattening droplets was standardized by three factors: (1) coverslips of the same mass were dropped on to threads from the same height, (2) the deflection of threads upon impact of the coverslips was controlled by the uniform length of the suspended thread spans, as determined by the equal spacing of thread sampler supports, and (3) the final force applied to the coverslip was set by the stiffness of the coverslip, the uniform width of the space into which a coverslip deformed when pressed by the probe and the uniform limit to downward movement of the probe, which was less than that required to break a coverslip.

We used ImageJ to measure the flattened surface area of each of the three droplets and of their glycoprotein cores. As an additional control for droplet flattening, we divided droplet volume by flattened droplet surface area to determine average flattened droplet thickness and used only the two droplets with the most similar thicknesses in subsequent computations. Flattened droplet measurements were not made at 72% RH for the first three *A. aurantia* studied, but were taken for all subsequent samples. *Neoscona crucifera* droplets were more viscous than those of *A. aurantia*. Consequently, we were unable to measure *N. crucifera* flattened areas at 20% RH and obtained measurements of only six individuals' threads at 37%. Glycoprotein could not be clearly resolved in the droplets of one *A. aurantia* individual at 90% RH or in the droplets of one *N. crucifera* individual at 55% and 72% RH.

For each RH we determined glycoprotein volume by multiplying the flattened area of a droplet's glycoprotein core by the droplet's average thickness. Subtracting glycoprotein volume from droplet volume yielded the volume of the droplet's outer, aqueous material. Because we could not both determine the volume of a droplet's glycoprotein core and extend this droplet, we inferred the volume of glycoprotein within an extended droplet by multiplying the droplet's volume by the mean glycoprotein volume-to-droplet volume ratio of the two flattened droplets of that individual's thread with the most similar droplet thicknesses. Indices of droplet extension per glycoprotein volume and relative stress on extended droplet filaments, as described below, were computed from a droplet's inferred glycoprotein volume, as this value was most closely associated with the droplet's performance.

We believe that this method provides a useful measure of glycoprotein volume. Nomarski images of flattened droplets show that the glycoprotein core extends above the level of the aqueous material (Fig. 5A). A side view of a 10 µl droplet of distilled water on glass shows the edges of the droplet to be tapered (Fig. 5B), a configuration that is consistent with that seen in a flattened droplet (Fig. 5A). Thus, a side view of a flattened droplet without its two axial fibers would be similar to the reconstruction in Fig. 5C. Actual glycoprotein volume is probably slightly greater than that determined from its surface area, although, after factoring out the volume of axial fibers passing through the glycoprotein, these two volumes should be similar. Increases in humidity appear to affect the flattened surface areas of glycoprotein and aqueous material in a similar manner. At higher humidity, glycoprotein plasticity increases and droplet cores probably flatten to a greater extent. At higher humidity, aqueous material becomes more dilute and less viscous and forms a thinner layer on the glass coverslip. Therefore, we believe that our method of determining glycoprotein volume was not biased by humidity level.

Indices of droplet performance

We computed two indices of droplet performance at each humidity: (1) extension per glycoprotein volume at pull-off (EGV) and (2) relative glycoprotein stress at pull-off (RGS). We computed EGV by dividing maximum droplet extension by glycoprotein volume. Values of this index increase as absorbed water makes glycoprotein more plastic, and decrease as absorbed water over-lubricates a droplet's contact footprint, allowing it to be pulled free with less force. Our instrument was not equipped with a load cell to allow us to directly measure the force on an extending droplet. Therefore, as the stiffness of these two species' axial fibers is similar (Young's modulus for *A. aurantia* E=0.009 GPa, *N. crucifera* E=0.010 GPa) (Sensenig et al., 2010), we inferred the force on a glycoprotein filament from the deflection of its supporting axial line, which we measured from the screen capture of the extended droplet immediately before pull-off using ImageJ (Fig. 4 and Fig. 6, angle A). Subtracting this axial line angle (Fig. 6, angle A) from 180 deg and dividing the result by 2 produces an angle (angle B, Fig. 6), whose sine is proportional to the force on the glycoprotein filament.

As noted previously, some droplets, predominantly droplets of *A. aurantia* extended at 72% and 90% RH, did not release from the probe until the axial lines had passed from the camera's field of view. In these cases, we measured axial line deflection in the last frame where axial line angle could be determined. At this point, the axial line angle of *A. aurantia* was nearly 180 deg, averaging 175 deg at 72% and 178 deg at 90%.

The RGS on an extended filament just prior to droplet pull-off was then determined by dividing either the relative force (or the humidity-corrected relative force, described below) by the cross-sectional area of the glycoprotein filament, determined by dividing glycoprotein volume by the length of the extended droplet at pull-off. Although RGS is not an engineering grade index, it does allow a general assessment and comparison of the two species' glycoproteins.

An issue that may impact the estimation of relative force at droplet pull-off is an apparent increase in axial fiber supercontraction as relative humidity rises. This phenomenon of supercontraction is well documented for dry dragline threads (Agnarsson et al., 2009; Blackledge et al., 2009; Boutry and Blackledge, 2010; Work, 1981),

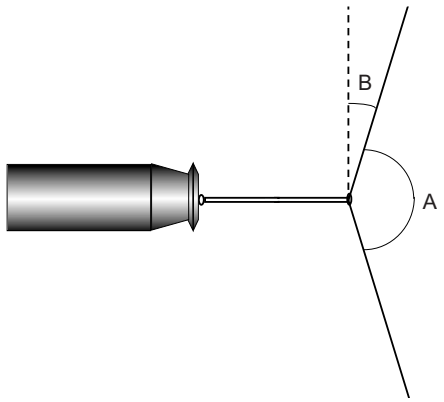

Fig. 6. An extended droplet showing angles A and B used to compute relative stress on the filament.

but has not been studied in viscous threads. Although it might appear that the already water-covered axial lines of viscous threads would not further supercontract, when immersed in water they do (Gosline et al., 1999) and become more taut. Three lines of evidence suggest that even humidity alters viscous thread supercontraction. (1) Videos of droplets extending at low humidities, particularly those of *N. crucifera* droplets, often showed the thread's axial line pair to be slack and sometimes convoluted as it flew back upon droplet release, whereas at higher humidities the supporting line remained taut. (2) As building humidity dropped, viscous threads in a few web samples showed some slackness, but became taut when gently exhaled upon, suggesting that water uptake increased supercontraction. (3) We placed four to six single droplet isolates on microscope slides so that we did not have to open the humidity chamber during a trial series. At low humidities these strands nearly always remained intact, but as humidity increased an increasing number of them spontaneously pulled from the adhesive holding them to the sampler's supports. We attribute this to two factors: increased supercontraction, which increases axial line tension, and increased water content of the thread's aqueous layer, which lubricates axial lines allowing them to be more easily pulled from the adhesive.

Interspecific differences in such supercontraction probably have only minor impacts on our estimates of the stress on glycoprotein filaments at pull-off and this phenomenon is tangential to the focus of our study. However, because supercontraction increases the tension on viscous threads, increased force is required to achieve the same angle of axial line deflection as humidity increases. In an attempt to account for this, we multiplied the sine of angle B by the humidity-specific, supercontraction multiplier values shown in Table 2. These correction factors describe an exponential increase in super contraction from zero at the lowest humidity (20% for *A. aurantia* and 37% for *N. crucifera*) to a factor of 2 at 90% RH. The values used for the two species differ because at 37% RH, *N. crucifera* droplets have just become pliable enough to respond in a manner similar to those of *A. aurantia* at 20% RH. These supercontraction-corrected relative stress values are reported in Table 2.

Analysis

We assembled, summarized and analyzed data using JMP (SAS Institute, Cary, NC, USA), considering $P \leq 0.05$ as significant. As a previous study determined that ambient humidity affects the volume and extensibility of whole viscous thread droplets (Opell et al., 2011a), this analysis capitalizes on the increased number of test humidities to compare the response curves of aqueous material, glycoprotein and glycoprotein-specific indices. If the mean value of a feature at each RH was normally distributed (as shown by Shapiro–Wilk *W*-tests with $P \geq 0.05$), we used ANOVA to test the differences in mean values; these results are presented in Figs 9–13. If the mean at one or more humidites was not normally distributed, we log-transformed data. In most cases the means then became normally distributed. In four cases (glycoprotein volume at 20% RH for *A. aurantia*, droplet extension at 20% RH for *A. aurantia* and 37% RH for *N. crucifera*, and all relative stress values of *A. aurantia* droplet filaments) mean values remained non-normal. For the first three indices we performed both ANOVA and Wilcoxon/Kruskall–Wallis tests of means. For the relative stress of *A. aurantia*, we used only a Wilcoxon test.

The curves that describe changes in droplet features over the five experimental humidities (e.g. Fig. 9A,B) are accompanied by the percentage change in mean values from those expressed at 20% RH for *A. aurantia* and 37% RH for *N. crucifera*, whose computation required a droplet to flatten (e.g. Fig. 9B). When possible, the mean

Table 2. Values used to compute the relative stress on *Argiope aurantia* and *Neoscona crucifera* glycoprotein filaments at droplet pull-off

	Argiope aurantia					*Neoscona crucifera*				
	20%	37%	55%	72%	90%	37%	55%	72%	90%
Angle A	144±5	162±5	174±3	175±2	177±1	149±3	144±4	134±3	141±7
Corrected sine angle B	0.337±0.048	0.186±0.053	0.075±0.034	0.072±0.033	0.050±0.017	0.263±0.022	0.389±0.039	0.612±0.033	0.647±0.116
Out of frame extensions (no.: mean angle)	0	1: 179	2: 177±3	4: 175±3	9: 178±0	0	0	3: 139±8	7: 162±8
Filament cross-sectional area (μm^2)	22.75±4.79	7.54±1.07	5.23±1.10	4.73±1.23	7.22±1.95	9.92±1.97	6.22±1.34	1.78±0.17	1.72±0.63
Relative stress	0.023±0.005	0.020±0.005	0.010±0.003	0.013±0.007	0.0050±0.001	0.035±0.008	0.084±0.019	0.239±0.026	0.319±0.063
Supercontraction multiplier	1	1.182	1.414	1.674	2	1	1.266	1.580	2
Corrected relative stress	0.023±0.005	0.024±0.006	0.014±0.005	0.021±0.012	0.009±0.003	0.035±0.008	0.107±0.024	0.378±0.042	0.637±0.126

Data for angle, area and stress are means (± 1 s.e.m.).

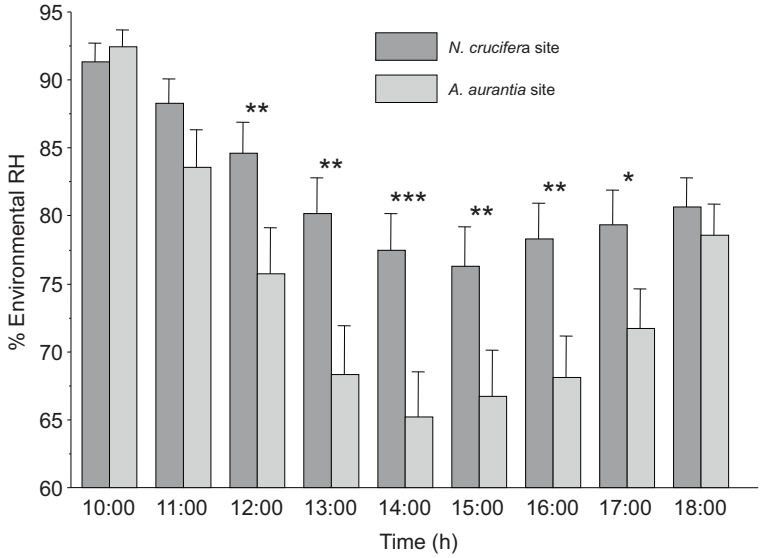

Fig. 7. Mean percentage RH (+1 s.e.m.) at the sites where *A. aurantia* and *N. crucifera* thread samples were collected, as recorded at 10 min intervals by Hobo data loggers during the 33 days that thread samples were collected for this study. *t*-test comparing the humidities of the two sites: *0.05<*P*<0.06, **0.01<*P*<0.05, ***P<0.01.

values at the five humidites were fitted to exponential or logarithmic curves, whose formulas are provided. When these curves did not adequately describe the values, polynomial curves were fitted. Below each feature of these figures we provide a histogram of the percentage maximum value of this feature, based on the greatest value expressed by both species (e.g. Fig. 9C,D).

RESULTS

From 11:00 h to 18:00 h, humidity was lower in the *A. aurantia* habitat than in the *N. crucifera* habitat, being significantly different from 12:00 h to 16:00 h (Fig. 7). Table 1 summarizes the volumes and extensibilities of droplets and Table 2 presents the values used to compute relative droplet stress. For *N. crucifera*, features computed from flattened droplet measurements were available only for 37% RH and greater, although values inferred for 20% RH from regression plots are given in brackets in Table 1 and included in the percentage histograms of Figs 9–13.

Across the five RH values the relationship between flattened droplet area (FDA) and flattened glycoprotein area (FGA) was similar for the two species (Fig. 8), showing that the species' droplets flattened in a similar manner and therefore would not bias our computation of glycoprotein volume in favor of one of the species. An insignificant effect of the interaction between FDA and species on FGA (P=0.58) showed that the slopes of the species' regressions did not differ. However, a significant contribution of species (P=0.0049) to the model 'FGA=FDA×species' showed that the *Y*-intercept of *A. aurantia* was greater than that of *N. crucifera*, as would be expected from the larger size of the former species' droplets (Fig. 1, Table 1).

With the exception of *N. crucifera* droplets measured at 37% RH, droplet volume increased as humidity increased, with *A. aurantia* droplets being more hygroscopic than *N. crucifera* droplets (Table 1). At 90% RH, *A. aurantia* droplets were 258.5±26.5% (mean ± s.e.m.) larger than at 20% RH, whereas *N. crucifera* droplets were only 160.6±8.5% larger at 90% than at 20% RH, a difference that was significant (*t*-test, P<0.0014). The aqueous component of both species' droplets increased as humidity increased (Table 1, Fig. 9). With the exception of *A. aurantia* droplets measured at 55% RH, glycoprotein volume increased as humidity increased (Table 1). At 37% and 55% RH, glycoprotein volume appeared to decrease or stabilize in both species (Fig. 10), although in *N. crucifera* the high variance and narrow range of values made this difficult to assess.

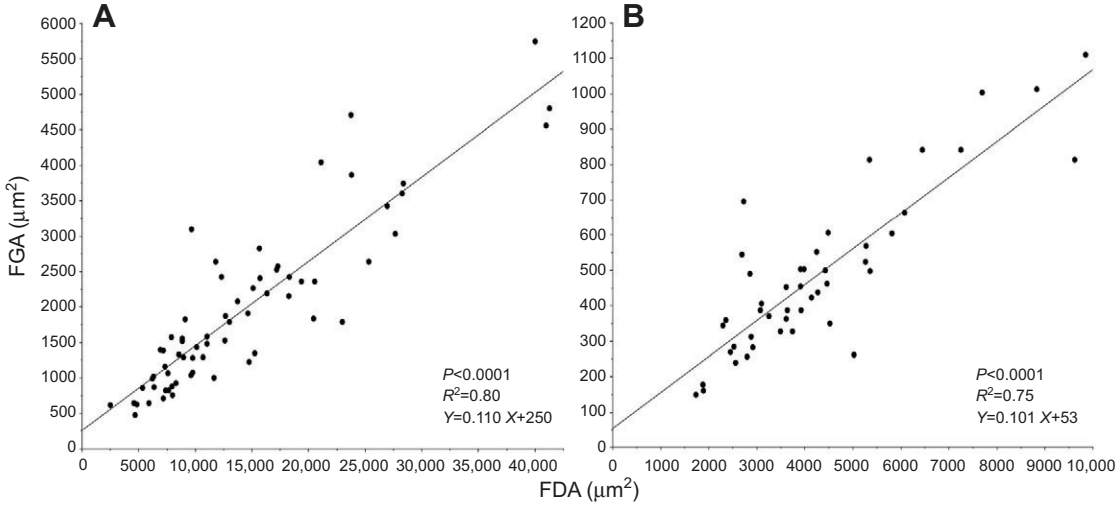

Fig. 8. Relationship between flattened droplet area (FDA) and flattened glycoprotein area (FGA) across the five experimental RH values for *A. aurantia* (A) and *N. crucifera* (B).

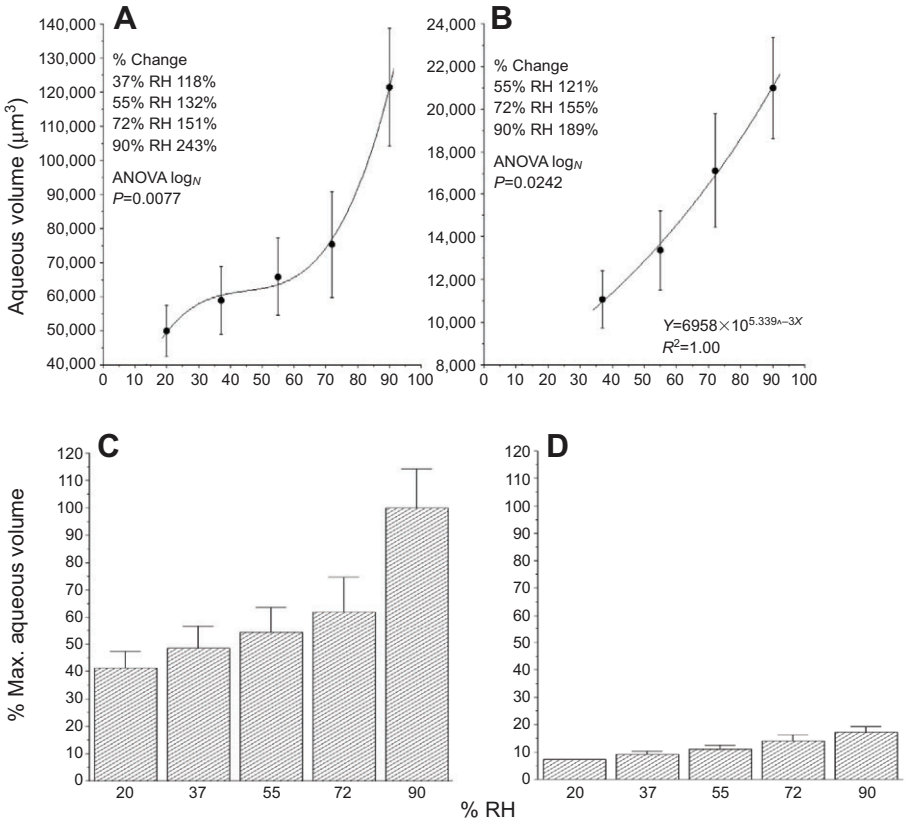

Fig. 9. Volume of a droplet's viscous material in *A. aurantia* (A,C) and *N. crucifera* (B,D) at five RH values (+1 s.e.m.). A and B present actual values, C and D the percentage maximum value expressed by both species.

When viewing Figs 9–13, which present the responses of viscous droplets to increasing humidity, it is useful to remember that viscous threads first experience high humidity during the early morning hours and humidity decreases as the day progresses. In each species, droplet extension increased with humidity, with the two species reaching similar pull-off lengths at 90% RH, despite the smaller volume of glycoprotein in *N. crucifera* droplets (Table 1, Fig. 11). However, the exponential increase in *N.*

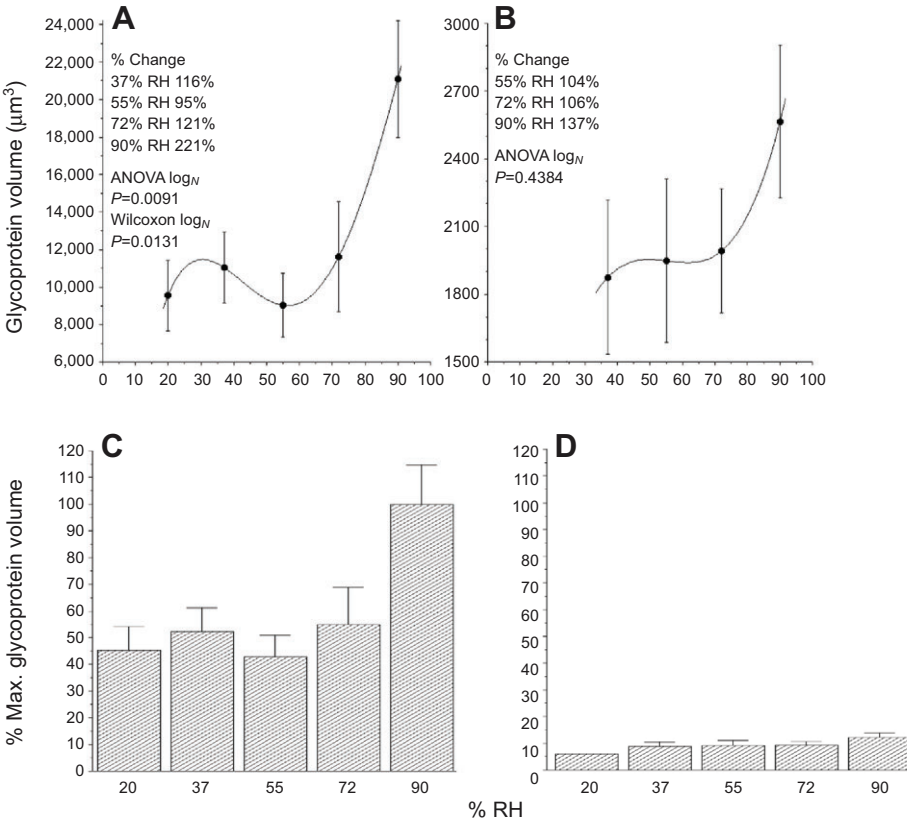

Fig. 10. Volume of a droplet's glycoprotein core in *A. aurantia* (A,C) and *N. crucifera* (B,D) at five RH values (±1 s.e.m.). A and B present actual values, C and D the percentage maximum value expressed by both species.

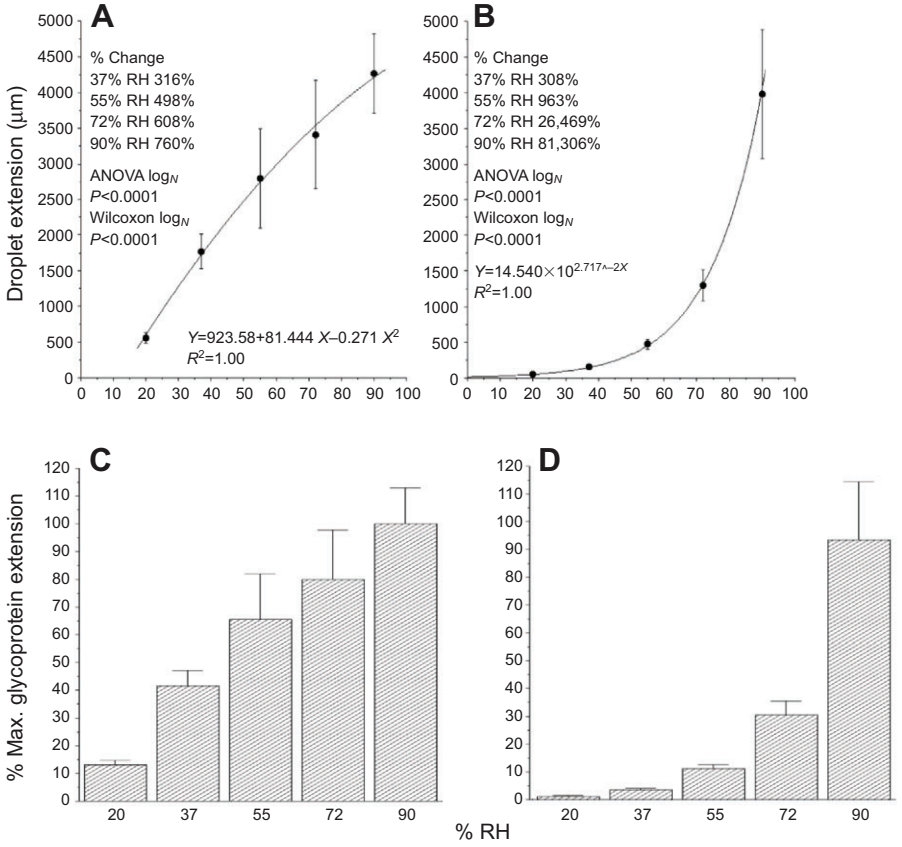

Fig. 11. Maximum extension of *A. aurantia* (A,C) and *N. crucifera* (B,D) droplets at five RH values (±1 s.e.m.). A and B present actual values, C and D the percentage maximum value expressed by both species.

crucifera droplet extension resulted in this species' droplet filaments being much shorter than those of *A. aurantia* at all other humidities.

Pronounced differences were observed in the two species' droplet EGV (Table 1, Fig. 12). In *A. aurantia*, EGV increased in a linear fashion from 20% to 55%, presumably as absorbed water increased

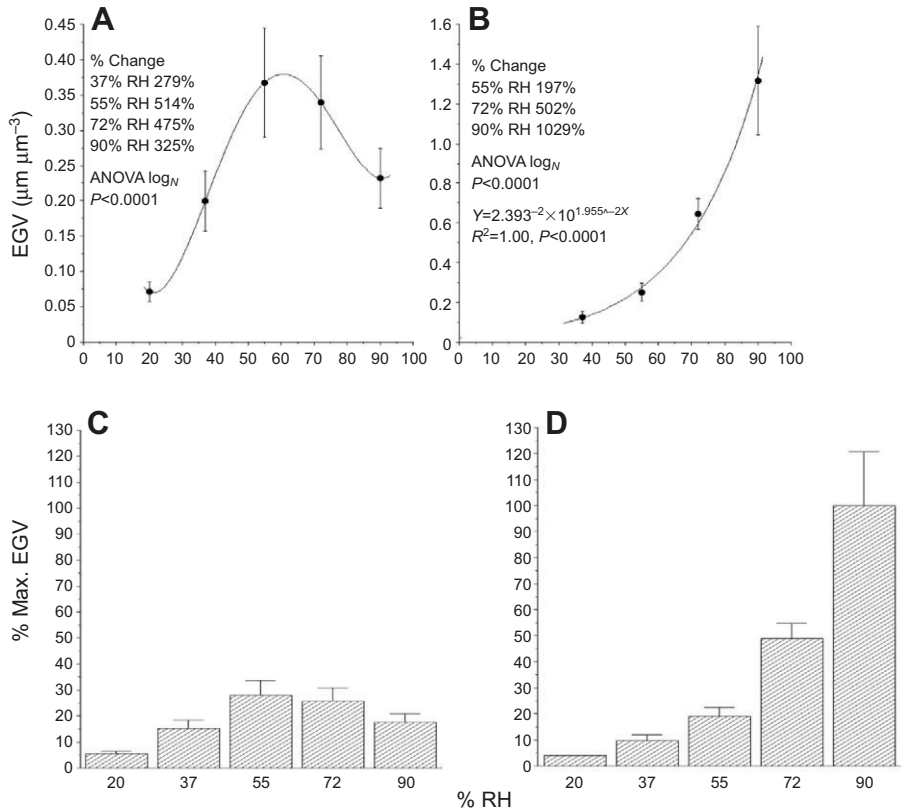

Fig. 12. Maximum droplet extension per glycoprotein volume (EGV) of *A. aurantia* (A,C) and *N. crucifera* (B,D) at five RH values (±1 s.e.m.). A and B present actual values, C and D the percentage maximum value expressed by both species.

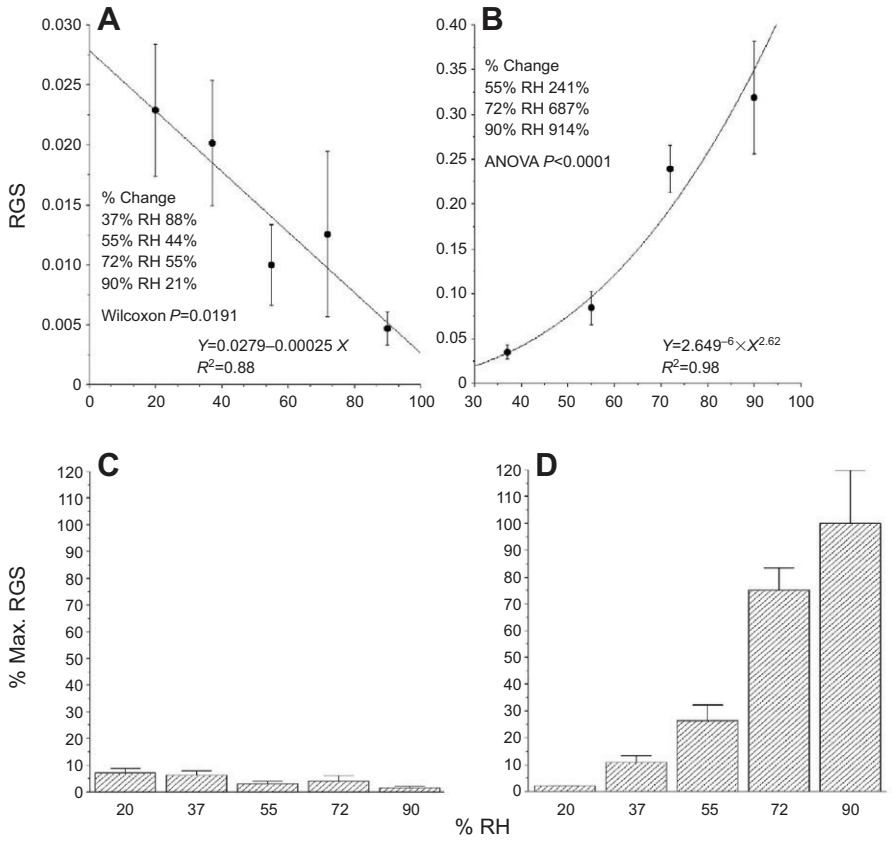

Fig. 13. Relative glycoprotein stress (RGS) on droplet filaments of *A. aurantia* (A,C) and *N. crucifera* (B,D) at maximum extension at five RH values (±1 s.e.m.). A and B present actual values, C and D the percentage maximum value expressed by both species.

glycoprotein plasticity, and then declined as droplets became over-lubricated and more easily released from the probe (Tukey HDS test rank, from low to high index values: 20%, 37%=90%, 55%=72%). In contrast, *N. crucifera* EGV values increased exponentially as humidity increased, reaching a maximum value at 90% RH that was 3.58 times the maximum value reached by *A. aurantia* at 55% RH.

In *A. aurantia*, uncorrected RGS just prior to pull-off decreased in a linear fashion as humidity increased, whereas RGS increased logarithmically in *N. crucifera* (Table 1, Fig. 13A,B), reaching a maximum value at 90% RH, 13.9 times the maximum value of *A. aurantia*, which was observed at 20% RH. When corrected for supercontraction, *A. aurantia* RGS did not differ among humidities (Wilcoxon χ^2, P=0.1582), whereas *N. crucifera* corrected RGS did (ANOVA, P<0.0001), increasing exponentially (Y=1.596^{-7}×$X^{3.39}$) and reaching a maximum value at 90% RH, 26.7 times the maximum value of *A. aurantia*, which was observed at 37% RH (Table 2).

DISCUSSION

Our results support the hypothesis that *A. aurantia* droplets are more hygroscopic than *N. crucifera* droplets, permitting them to remain hydrated and perform optimally, and adapting them to drier environments and times of the day. However, like droplets of *L. cornutus* (Sahni et al., 2011), those of *A. aurantia* become progressively over-lubricated at RH greater than 55%, resulting in decreased EGV (Fig. 12A,C, Fig. 14). In contrast, the EGV of *N.*

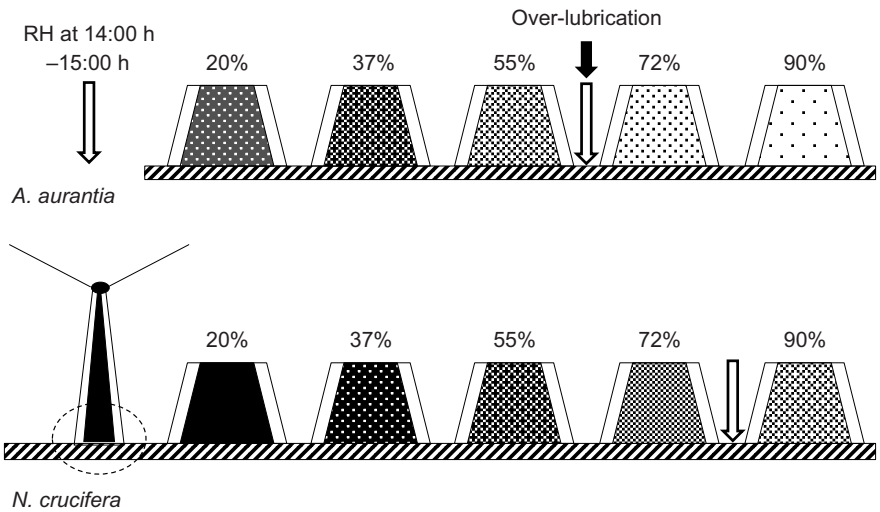

Fig. 14. Hydration of glycoprotein in the footprints of *A. aurantia* and *N. crucifera* droplets at experimental RH values and its relationship with low mid-afternoon humidities in the two species' environments. Lighter shading reflects greater glycoprotein water content.

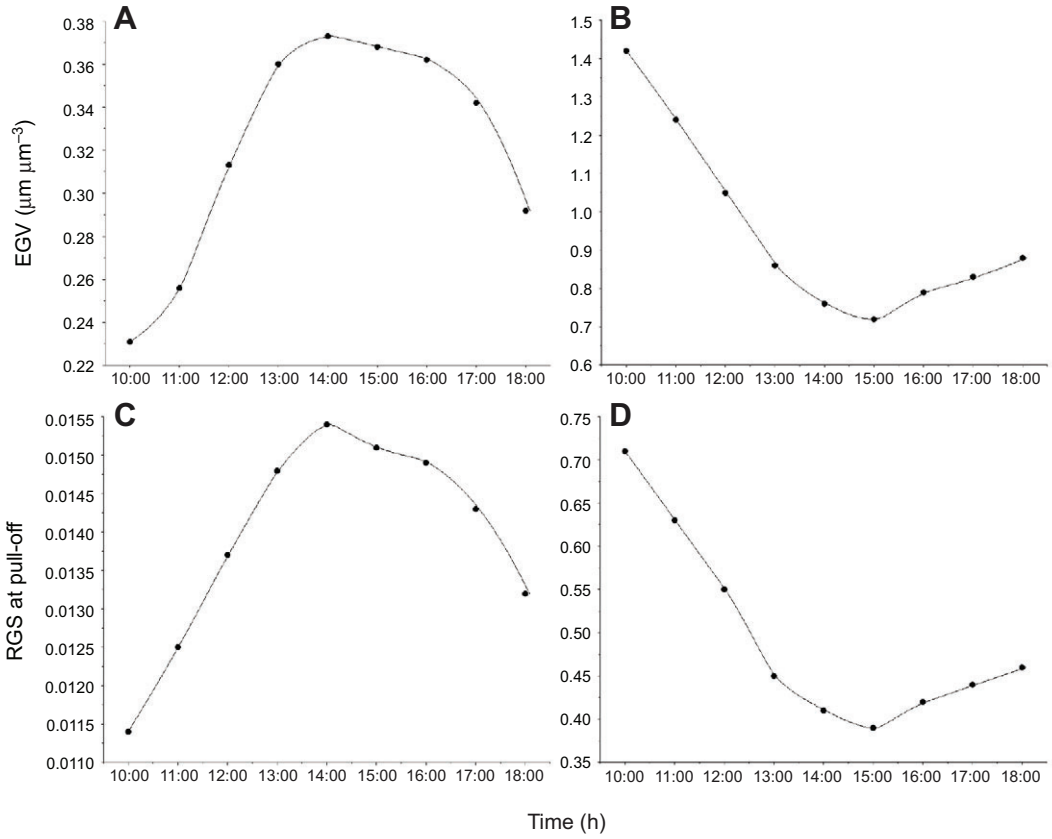

Fig. 15. Changes in EGV and RGS at droplet pull-off (corrected for the effect of RH on axial line supercontraction) of *A. aurantia* (A,C) and *N. crucifera* (B,D) droplets from mid-morning to late afternoon during the course of this study.

crucifera increased exponentially as humidity increased, and showed no evidence of over-lubrication (Fig. 12B,D, Fig. 14). The lower hygroscopicity of *N. crucifera* droplets also caused their glycoprotein to remain more viscoelastic at higher humidity, resulting in an exponential increase in the relative stress on the glycoprotein filaments at pull-off (RGS) as humidity increased (Fig. 13B,D). This contrasts with the low and decreasing RGS of *A. aurantia* droplets as RH increased. As RGS is an indicator of the energy required to extend a droplet to pull-off, this suggests that increased humidity enhances the ability of *N. crucifera* threads to absorb the energy of struggling prey through extension, whereas it has a negative effect on the ability of *A. aurantia* threads to absorb energy in this manner.

These interspecific differences in EGV and RGS are consistent with the hypothesized environmental adaptiveness of droplet hygroscopicity. At 14:00 h–15:00 h, when the humidity of both species' habitats was at its lowest (Fig. 7), RH in the *A. aurantia* habitat dropped to a mean of 66% and in the *N. crucifera* habitat to 76%. For *A. aurantia*, this low humidity mark corresponds with the humidity range at which droplets have reached their maximum EGV and just begin to show signs of over-lubrication (Fig. 12A,C, Fig. 14). In contrast, at times of lowest daily RH, *N. crucifera* droplets exhibited only half of their maximum EGV (Fig. 12B,D) and over half of their maximum RGS (Fig. 13B,D). Consequently, when differences in EGV and supercontraction corrected RGS are examined from mid morning to late afternoon (10:00 h–18:00 h), *A. aurantia* droplets exhibited their maximum values during mid afternoon and *N. crucifera* during the morning (Fig. 15). Thus, hygroscopic differences in the two species' viscous threads appear to adapt them to function optimally not only in different humidity regimes (Fig. 14) but also at different times of the day (Fig. 15). However, it is important to note that the minimum midday EGV of *N. crucifera* was 1.9 times the maximum value for *A. aurantia* and that the minimum midday RGS of *N. crucifera* was 23 times the maximum value for *A. aurantia*.

As a biomimetic system, *N. crucifera* droplets appear to offer more promise than *A. aurantia* droplets because *N. crucifera* EGV and RGS increase exponentially and logarithmically, respectively, as RH increases (Fig. 11B, Fig. 12B, Fig. 13B). Moreover, *N. crucifera* droplets attain a maximum EGV that is 3.6 times that of *A. aurantia* and an RGS at 90% RH that is 64 times that of *A. aurantia* at 90% RH. However, *A. aurantia* droplets illustrate how an adhesive system might be engineered to fail at a desired humidity. The simplest explanation for these interspecific differences is that the aqueous material of *A. aurantia* is more hygroscopic than that of *N. crucifera* as a result of having more and/or different low molecular weight compounds. *Argiope aurantia* glycoproteins may also be more hygroscopic, causing them to take up a higher percentage of the atmospheric water provided by the aqueous material and, thereby, become more extensible at a given RH than the glycoprotein within *N. crucifera* droplets.

Although it is convenient to attribute increased droplet extensibility at higher humidities to the dilution of glycoprotein by absorbed atmospheric water, this may be an oversimplification given the complex interactions that establish the three-dimensional configuration of glycoproteins. Intramolecular hydrogen bonding establishes most of the directional interactions that underpin protein folding. However, the burial of hydrophobic (apolar) side-chains within the molecule plays a key role in organizing and stabilizing the folded molecule (Rose, 1993; Bolen and Rose, 2008). Residues within these buried hydrophobic regions are themselves configured by hydrogen bonding. Poor osmolytes, like water, disrupt intramolecular hydrogen bonding and suppress secondary structure because the strength of these bonds is weakened by competition with water molecules that supply alternative bonding sites, thereby

reducing hydrogen bonding as water content increases. These structural changes may increase glycoprotein unfolding as humidity increases. Moreover, increased water content may also cause additional apolar groups to be forced to the molecule interior, a change that is associated with increased entropy and volume (Dill, 1990). The decrease in glycoprotein flattened area and volume observed at 55% RH in *A. aurantia* and the probable stabilization of *N. crucifera* glycoprotein flattened area and volume at intermediate humidities (Table 1, Fig. 10A,B) may reflect such changes in molecular configuration.

This study shows that a single model cannot explain the performance of viscous threads produced by all orb-weavers and suggests that the environmental responsiveness of these threads has been shaped by natural selection. A full understanding of viscous thread evolution and operation will require investigations that characterize this diversity and address the impact of web environment on a viscous thread's molecular structure, material properties and prey capture performance.

ACKNOWLEDGEMENTS

Mary Lee Hendricks and Sarah Stellwagen provided useful comments on the manuscript.

AUTHOR CONTRIBUTIONS

B.D.O. designed and constructed the instrumentation used in this study, conceived the experiment, collected and prepared viscous threads for study, regulated chamber humidity, and performed most of the droplet flattening procedures. S.E.K. and M.A.S. photographed stationary droplets, performed droplet extensions and video recording, analyzed still and video images, entered data and assisted with its preliminary analysis, and collaborated on an early draft of this manuscript. B.D.O. conducted the final analyses, prepared figures, and finalized the manuscript.

COMPETING INTERESTS

No competing interests declared.

FUNDING

Funds from the State Council for Higher Education for Virginia provided the digital camera used in this study.

REFERENCES

Adams, M. R. (2000). Choosing hunting sites: web site preferences of the orb weaver spider, *Neoscona crucifera*, relative to light cues. *J. Insect Behav.* **13**, 299-305.

Agnarsson, I. and Blackledge, T. A. (2009). Can a spider web be too sticky? Tensile mechanics constrains the evolution of capture spiral stickiness in orb weaving spiders. *J. Zool.* **278**, 134-140.

Agnarsson, I., Boutry, C., Wong, S.-C., Baji, A., Sensenig, A. and Blackledge, T. A. (2009). Supercontraction forces in spider dragline silk depend on rate of humidity change. *Zoology* **112**, 325-331.

Blackledge, T. A. and Zevenbergen, J. M. (2006). Mesh width influences prey retention in spider orb webs. *Ethology* **112**, 1194-1201.

Blackledge, T. A., Boutry, C., Wong, S. C., Baji, A., Dhinojwala, A., Sahni, V. and Agnarsson, I. (2009). How super is supercontraction? Persistent *versus* cyclic response to humidity in spider dragline silk. *J. Exp. Biol.* **212**, 1981-1989.

Bolen, D. W. and Rose, G. D. (2008). Strucutre and energetics of hydrogen-bonded backbone in protein folding. *Ann. Rev. Biochem.* **77**, 339-362.

Boutry, C. and Blackledge, T. A. (2010). Evolution of supercontraction in spider silk: structure-function relationship from tarantulas to orb-weavers. *J. Exp. Biol.* **213**, 3505-3514.

Carrel, J. (2008). The effect of season of fire on density of female garden orbweavers (Araneae: Araneidae: Argiope) in Florida crub. *Fla. Entomol.* **91**, 332-334.

Chacón, P. and Eberhard, W. G. (1980). Factors affecting numbers and kinds of prey caught in artificial spider webs with considerations of how orb-webs trap prey. *Bull. Br. Arachnol. Soc.* **5**, 29-38.

Choresh, O., Bayarmagnai, B. and Lewis, R. V. (2009). Spider web glue: two proteins expressed from opposite strands of the same DNA sequence. *Biomacromolecules* **10**, 2852-2856.

Coddington, J. A. (1989). Spinneret silk spigot morphology: evidence for the monophyly of orb-weaving spiders, Cyrtophorinae (Araneidae), and the group Theridiidae plus Nesticidae. *J. Arachnol.* **17**, 71-96.

Dill, K. A. (1990). Dominant forces in protein folding. *Biochemistry* **29**, 7133-7155.

Edmonds, D. and Vollrath, F. (1992). The contribution of atmospheric water vapour to the formation and efficiency of a spider's web. *Proc. R. Soc.* **248**, 145-148.

Edwards, G. B. (1984). Large Florida orb-weavers of the genus *Neoscona*. *Entomology Circular, Florida Department of Agriculture and Consumer Services* **266**, 1-2.

Elbaum, R., Zaltzman, L., Burgert, I. and Fratzl, P. (2007). The role of wheat awns in the seed dispersal unit. *Science* **316**, 884-886.

Enders, F. (1977). Web-site selection by orb-web spiders, particularly *Argiope aurantia* Lucas. *Anim. Behav.* **25**, 694-712.

Fischer, F. G. and Brander, J. (1960). Eine analyse der gespinste der kreuzspinne. *Hoppe-Seyler's Z. Physiol. Chem.* **320**, 92-102.

Gosline, J. M., Guerette, P. A., Ortlepp, C. S. and Savage, K. N. (1999). The mechanical design of spider silks: from fibroin sequence to mechanical function. *J. Exp. Biol.* **202**, 3295-3303.

Gosline, J. M., Pollak, C. C., Guerette, P. A., Cheng, A., DeMont, M. E. and Denny, M. W. (1993). Elastomeric network models for the frame and viscid silks from the orb web of the spider *Araneus diadematus*. In *Silk Polymers: Materials Science and Biotechnology*, American Chemical Society Symposium Series 544 (ed. D. Kaplan, W. W. Adams, B. Farmer and C. Viney), pp. 328-341. *Polym. Adv. Technol.* 6:717. doi:10.1002/pat.1995.220061107.

Higgins, L. E., Townley, M. A., Tillinghast, E. K. and Rankin, M. A. (2001). Variation in the chemical compositon of orb webs built by the spider *Nephila clavipes* (Araneae, Tetragnathidae). *J. Arachnol.* **29**, 82-94.

Opell, B. D. and Hendricks, M. L. (2007). Adhesive recruitment by the viscous capture threads of araneoid orb-weaving spiders. *J. Exp. Biol.* **210**, 553-560.

Opell, B. D. and Hendricks, M. L. (2009). The adhesive delivery system of viscous capture threads spun by orb-weaving spiders. *J. Exp. Biol.* **212**, 3026-3034.

Opell, B. D. and Hendricks, M. L. (2010). The role of granules within viscous capture threads of orb-weaving spiders. *J. Exp. Biol.* **213**, 339-346.

Opell, B. D. and Schwend, H. S. (2007). The effect of insect surface features on the adhesion of viscous capture threads spun by orb-weaving spiders. *J. Exp. Biol.* **210**, 2352-2360.

Opell, B. D., Karinshak, S. E. and Sigler, M. A. (2011a). Humidity affects the extensibility of an orb-weaving spider's viscous thread droplets. *J. Exp. Biol.* **214**, 2988-2993.

Opell, B. D., Tran, A. M. and Karinshak, S. E. (2011b). Adhesive compatibility of cribellar and viscous prey capture threads and its implication for the evolution of orb-weaving spiders. *J. Exp. Zool.* **315**, 376-384.

Peters, H. M. (1986). Fine structure and function of capture threads. In *Ecophysiology of Spiders* (ed. W. Nentwig), pp. 187-202. New York, NY: Springer Verlag.

Puthoff, J. B., Prowse, M. S., Wilkinson, M. and Autumn, K. (2010). Changes in materials properties explain the effects of humidity on gecko adhesion. *J. Exp. Biol.* **213**, 3699-3704.

Rasband, W. S. (1997-2012). *ImageJ*. USA National Institutes of Health, Bethesda, MD. http://imagej.nih.gov/ij/

Rose, G. D. (1993). Hydrogen bonding, hydrophobicigty, packing, and protein folding. *Ann. Rev. Biophys. Biomol. Str.* **22**, 381-415.

Sahni, V., Blackledge, T. A. and Dhinojwala, A. (2010). Viscoelastic solids explain spider web stickiness. *Nat. Commun.* **1**, 19.

Sahni, V., Blackledge, T. A. and Dhinojwala, A. (2011). Changes in the adhesive properties of spider aggregate glue during the evolution of cobwebs. *Sci. Rep.* **1**, 41.

Sensenig, A., Agnarsson, I. and Blackledge, T. A. (2010). Behavioural and biomaterial coevolution in spider orb webs. *J. Evol. Biol.* **23**, 1839-1856.

Tillinghast, E. K. and Christenson, T. E. (1984). Observations on the chemical composition of the web of *Nephila clavipes* (Araneae, Araneidae). *J. Arachnol.* **12**, 69-74.

Tillinghast, E. K., Townley, M. A., Wight, T. N., Uhlenbruck, G. and Janssen, E. (1993). The adhesive glycoprotein of the orb web of *Argiope aurantia* (Araneae, Araneidae). In *Proceedings* of the *Materials Research Society Symposium* **292**, 9-23.

Townley, M. A., Bernstein, D. T., Gallanger, K. S. and Tillinghast, E. K. (1991). Comparative study of orb-web hydroscopicity and adhesive spiral composition in three areneid spiders. *J. Exp. Zool.* **259**, 154-165.

Townley, M. A., Tillinghast, E. K. and Neefus, C. D. (2006). Changes in composition of spider orb web sticky droplets with starvation and web removal, and synthesis of sticky droplet compounds. *J. Exp. Biol.* **209**, 1463-1486.

Vollrath, F. (1992). Spider webs and silks. *Sci. Am.* **266**, 70-76.

Vollrath, F., Fairbrother, W. J., Williams, R. J. P., Tillinghast, E. K., Bernstein, D. T., Gallagher, K. S. and Townley, M. A. (1990). Compounds in the droplets of the orb spider's viscid spiral. *Nature* **345**, 526-528.

Work, R. W. (1981). A comparative study of the supercontraction of major ampullate spider fibers of orb-weaving spiders (Araneae). *J. Arachnol.* **9**, 299-308.

Young, O. P. and Edwards, G. B. (1990). Spiders in United States' field crops and their potential effect on crop pests. *J. Arachnology* **18**, 1-27.